Determination of the Intracranial Volume: A Registration Approach

Sven Hentschel and Frithjof Kruggel

Interdisziplinäres Zentrum für Klinische Forschung (IZKF),
Inselstrasse 22, D-04103 Leipzig, Germany
kruggel@cbs.mpg.de

Abstract. An algorithm to segment the intracranial compartment from PD-weighted MR images of the human head is described. If only a T_1-weighted dataset is available for a given subject, an artifical PD-weighted dataset is computed from a dual-weighted reference by non-linear registration of the T_1-weighted datasets, and the intracranial compartment is segmented from this artificial dataset. The performance of the algorithm is evaluated on the basis of 12 dual-weighted datasets with an average volume difference of 2.05% and an average overlap (Dice index) of 0.968.

1 Introduction

Skull growth occurs along the suture lines and is determined by brain expansion, which takes place during the normal growth of the brain [9], [19]. Thus in normal adults, a close relationship between the brain size and the intracranial volume (ICV) is expected. This relationship is used to estimate the premorbid brain size in degenerative brain diseases (e.g., Alzheimer's disease [7], [11], [21]) or brain degeneration due to diffuse or focal brain damage.

Three major approaches were suggested to determine the ICV from images of the head: (a) manual delineation of the intracranial compartment in CT [1], [10], [18] or MR images [7], [8], (b) classification and segmentation of multispectral MR images [2], [3], [4], and (c) classification and segmentation of T_1-weighted MR images [15], [16]. While a manual delineation is certainly laborious, the second approach requires the acquisition of multispectral volume images, which is often too time consuming (and thus, too costly) to be acceptable for routine clinical studies. The third method, using T_1-weighted images only, makes certain assumptions that are invalid at least for datasets acquired by our imaging protocol.

Our approach is based on the idea that proton-density (PD)-weighted MR images provide a good basis for ICV segmentation, because the skull signal intensity is low, and all intracranial tissue and the cerebrospinal fluid (CSF) provide a high signal intensity. Thus, the first part of our algorithm consists of generating an ICV mask from a PD-weighted MR image. Most often, only a high-resolution T_1-weighted MR image is available. So the second part of our algorithm consists of a non-linear registration of a T_1-weighted reference image to a T_1-weighted study image, yielding a field of inter-subject deformation vectors. This deformation field is applied to the PD-weighted

G.-Z. Yang and T. Jiang (Eds.): MIAR 2004, LNCS 3150, pp. 253–260, 2004.

reference image to generate an "artificial" PD-weighted study image. This artificial PD-weighted image is finally segmented to yield an ICV mask for the study image.

In the next section, we describe our approach in more detail. Then, we evaluate its performance in a "bootstrap" fashion. Finally, we compare our method and results with the three approaches mentioned above.

2 Algorithms

In the following, certain heuristics (detailed below) require that the dataset has been aligned with the stereotactic coordinate system. The x axis corresponds to the ear-to-ear direction, the y axis to the nose-to-back direction, the z axis to the head-to-feet direction. Indices ca resp. cp refer to the position of the anterior and posterior commissure.

2.1 Generating an ICV Mask from a PD-weighted MR Image

On input, we expect a PD-weighted image of a human head at an isotropical resolution of 1 mm and an intensity resolution of 256 steps. Intensity inhomogeneities should have been corrected by any suitable algorithm. Note that the dataset has been aligned with the stereotactic coordinate system, e.g., by registration with an aligned T_1-weighted image of the same subject. The algorithm consists of three steps: (a) computation of a head mask, (b) computation of an initial ICV mask, (c) refinement of the ICV mask at the brainstem and hypophysis.

Computation of a head mask: The aim is to segment the head region as a single connected component without holes. Steps are spelled out as follows:

$i_1 = \text{isodata}(i_{PD}, 2)$ // segment into two intensity classes
$i_2 = \text{binarize}(i_1, 1, 1)$ // select foreground voxels
$i_3 = \text{dilate}(i_2, 5)$ // morphological dilation by 5mm
$i_4 = \text{invert}(i_3)$ // next 3 steps fill holes inside head mask
$i_5 = \text{selectBig}(\text{label}(i_4, 26))$ // select biggest 26-connected component
$i_6 = \text{invert}(i_5)$
$i_7 = \text{erode}(i_6, 5)$ // restore original head size
$i_{hm} = \text{selectBig}(\text{label}(i_7, 26))$ // select the biggest component

Computation of an initial ICV mask: The next step is to generate a first mask of the intracranial region. The threshold th and eroding distance $dist$ are determined iteratively:

$i_1 = \text{erode}(i_{hm}, 5)$ // erode head mask by 5mm
$i_{ext} = \text{invert}(i_1)$ // this mask contains all exterior voxels
$th = 40, dist = 4$ // set initial parameters
do {
  $i_2 = \text{binarize}(i_{PD}, th, 255)$ // select voxels above an intensity threshold
  $i_3 = \text{erode}(i_2, dist)$ // separate ICV from small components
  $i_4 = \text{selectBig}(\text{label}(i_3, 26))$ // select biggest 26-connected component
  $i_{icv1} = \text{dilate}(i_4, dist)$ // restore original mask size
  th += 5, $dist$ += 0.6 // increment parameters
} while $(\text{and}(i_{icv1}, i_{ext}) \neq \{\})$ // stop if exterior and ICV mask do not overlap

Due to the application of morphological operators with large kernels, some areas of the intracranial volume with high curvature are rounded off in this first mask. A refinement step adds these voxels back:

$i_1 = \text{dilate}(i_{icv1}, 2)$ // dilate ICV mask by 2mm
$i_2 = \text{mask}(i_1, i_{PD})$ // mask out these voxels from the PD image
$i_3 = \text{binarize}(i_2, th, 255)$ // select voxels above an intensity threshold
$i_4 = \text{and}(\text{invert}(i_{ext}), i_1)$ // select only voxels above an intensity threshold...
$i_5 = \text{open}(\text{and}(i_3, i_4), 1)$ // ...that do not belong to the exterior mask
$i_{icv2} = \text{selectBig}(\text{label}(i_5, 26))$ // select biggest 26-connected component

Computation of the final ICV mask: The brainstem and hypophysis regions need special treatment, because here the high flow in large vessels and CSF lead to a low signal in the PD-weighted image. Thus, parts in these areas are not included in the initial ICV mask.

Fig. 1. Refinement of brainstem segmentation: Midsagittal plane of image i_{cone} (left), after thinning (middle), and brainstem midline (right).

Refinement at the brainstem: A cone-shaped mask is placed with a tip at the center of the anterior and posterior commissure, and a basis at the bottommost slice of the dataset with a maximum radius of 80mm. Voxels of the PD-weighted image within this mask are selected if their intensity is above 100 to yield the binary image i_{cone} (see Fig. 1). The medial surfaces of the objects in this image are computed [20]. Sagittal slices in this datasets are searched for the longest connected line that is denoted as the brainstem midline.

Using this line, the brainstem and its surrounding CSF is segmented sequentially in axial slices. In each slice, the smallest distance d_h from the midline voxel v_m to the next background voxel is determined. All foreground voxels within the circle of radius d_h around v_m are collected as the initial brainstem mask i_{bs}. This mask is dilated by 10mm to yield i_{bs_10}. In this mask i_{bs_10}, each foreground voxel is visited radially, starting from the midline voxel. A foreground voxel is eliminated if one of the following conditions is true: (a) this voxel belongs to the background in i_{PD}, (b) we approached the dura mater around the brainstem: this voxel does not belong to the brainstem in i_{bs}

and has an intensity above 80 in i_{PD}, (c) condition (a) or (b) were already true on the radial path.

Finally, a morphological opening using a 1.5mm kernel and a selection of the biggest connected component leads to the brainstem mask that is joined with i_{icv2} to yield i_{icv3}.

Refinement at the hypophysis: In the aligned images, the position of the hypophysis is well known within the subvolume ($x_{ca} - 20 \leq x \leq x_{ca} + 20$, $y_{ca} - 20 \leq y \leq y_{cp}$, $z_{ca} \leq y \leq 160$). Voxels within this subvolume above the threshold th of i_{PD} are collected as image i_{hy}. Now, the region around the hypophysis is segmented as follows:

$i_1 = \mathrm{and}(\mathrm{invert}(i_{icv3}), i_{hy})$	// remove voxels that already belong to i_{icv}
$i_2 = \mathrm{open}(i_1, 1)$	// remove small bridges to the hypophysis
$i_3 = \mathrm{selectBig}(\mathrm{label}(i_2, 26))$	// select the hypophysis
$i_4 = \mathrm{or}(i_3, i_{icv})$	// join the hypophysis with i_{icv}
$i_{icv4} = \mathrm{close}(i_4, 5)$	// close small gaps

Finally, starting from the bottommost axial slice in image i_{icv4} upwards, the area of the ICV mask is calculated. A running average is computed over 10 slices; the level z_{cer} at which the current value is greater than 2 times the running average is taken as the basis of the cerebellum [15]. Voxels in axial slices below $z_{cer} + 10$ are removed to yield the final ICV mask i_{icv} (see Fig. 2).

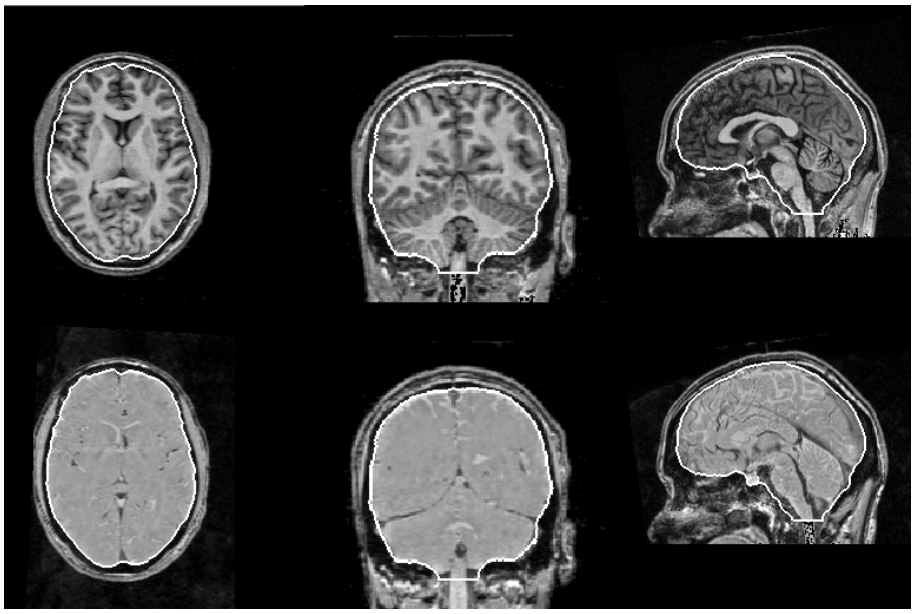

Fig. 2. Border of the ICV mask overlaid on the T_1-weighted image (top row) resp. PD-weighted image (bottom row) for reference sample 12 (see below).

This algorithm was implemented in C++ using the BRIAN environment [12]. The computation time is 221s (AMD Athlon 1800+ machine, Linux 2.4 operating system).

2.2 Generating an Artificial PD-weighted Image

Given reference datasets i_{T1_ref} and i_{PD_ref}, an artificial PD-weighted image i_{PD_stu} for a study subject is computed using i_{T1_stu}. A non-linear registration from i_{T1_ref} onto i_{T1_stu} yields a field of deformation vectors i_{def}. In principle, any method for non-linear registration may be used here that accomodates large-scale deformations. We used an approach based on fluid dynamics [5], [23]. The deformation field i_{def} is applied to the reference dataset i_{PD_ref} to yield an artificial PD-weighted image i_{PD_stu}. Our registration algorithm was implemented in C++ using the BRIAN environment, the computation time is about 22min (due to image dependent optimization, measured on an AMD Athlon 1800+ machine, Linux 2.4 operating system).

In summary, if T_1- and PD-weighted datasets are available for the same subject, an ICV mask is generated using the first algorithm. If only a T_1-weighted dataset is available, an artifical PD-weighted dataset is computed from a dual-weighted reference by non-linear registration, and an ICV mask is segmented from this artificial dataset.

3 Evaluation

Subjects: The MPI maintains a database of subjects enrolled for functional MRI experiments. Before admission, a brief history and physical inspection is taken by a physician. Subjects are included in this database if they comply with the informed consent for conducting general fMRI experiments, pass the examination and do not exhibit pathological features (e.g., unilateral ventricular enlargements, subarachnoidal cysts) in their MR tomograms. Twelve subjects were selected, for which high-resolution T_1- and PD-weighted datasets were available, generally acquired in separate sessions.
Image Acquisition: Magnetic resonance imaging (MRI) was performed on a Bruker 3T Medspec 100 system, equipped with a bird cage quadrature coil. T_1-weighted images were acquired using a 3D MDEFT protocol [14]: FOV 220×220×192 mm, matrix 256×256, 128 sagittal slices, voxel size 0.9×0.9 mm, 1.5 mm slice thickness, scanning time 15 min. PD-weighted images were acquired using a 3D FLASH protocol with the same resolution parameters.
Preprocessing: T_1-weighted images were aligned with the stereotactical coordinate system [13] and interpolated to an isotropical voxel size of 1 mm using a fourth-order b-spline method. Data were corrected for intensity inhomogeneities by a fuzzy segmentation approach using 3 classes [17]. PD-weighted images were registered with the aligned T_1-weighted images (6-parameter transformation for rotation and translation, normalized mutual information cost function, simplex optimization algorithm). Finally, the registered PD-weighted images were corrected for intensity inhomogeneities using 2 classes.
Processing: Data of one subject were considered as a reference. Artificial PD-weighted images were computed for the other 11 subjects by the method described above. ICV

	1	2	3	4	5	6	7	8	9	10	11	12
ΔV	1.68	1.82	2.03	2.11	3.54	2.25	1.93	1.73	2.14	1.46	2.73	1.23
dc	0.969	0.970	0.966	0.967	0.962	0.961	0.971	0.964	0.968	0.972	0.969	0.971

Table 1. Averaged volume differences ΔV (in percent) and overlap dc (Dice similarity index) for each reference vs. the 11 study subjects.

masks were determined from the real and the artifical PD-weighted images. Their volume differences ΔV (in percent) and overlap dc (as measured by the Dice similarity index [6]) were computed. So in total, 12 by 11 comparisons were made. Note that a low volume difference ($< 2\%$) and a high Dice index (> 0.96) correspond to a good adaptation of the ICV mask. Averaged results for each reference are compiled in Table 1. The volume difference ranged between 0.02% and 8.69%, the Dice index between 0.934 and 0.981. Best results were achieved if using sets 10 or 12 as reference.

Results Discussion: Although the algorithm may appear complex at first sight, it requires a set of only 10 basic image processing operations. The validity of the built-in anatomical heuristics were carefully checked for our database, and are expected to be valid for any (normal) MR image of the head.

Several factors influence the ICV segmentation: (a) The quality of the reference datasets. Head motion, flow and DC artifacts impede good segmentation results. (b) A high flow in the sinuses may lead to a low signal at the border of the intracranial cavity in the PD-weighted image, leading to possible segmentation errors at the ICV border. However, the induced volume error was found to be less than 0.5%. (c) In areas of the convexity of the skull where the tabula interna is very thin, the partial volume effect may smear the signal intense dura mater with the bone marrow, so that parts of the bone marrow are included in the ICV mask. Again, only a small induced volume error (0.2%) was found. In summary, the ICV mask should be checked visually when selecting datasets as a reference.

Other factors influence the adaptation quality of the artificial ICV mask: (a) We noted a significant relation between the volume difference ΔV before and after registration, e.g. a difference in the ICV volume between the reference and the study of 200ml leads to a volume error ΔV of 40ml (or 3%) in the artificial ICV mask. Most likely, this is a consequence of the partial volume effect in the registration procedure, since the ICV border layer has a volume of typically 65ml. (b) One may ask whether the deformation field generated from a non-linear registration of T_1-weighted datasets is a good model for the anatomical inter-subject differences, and thus suitable for applying it to the PD-weighted dataset. In particular, this is true for study cases where we found a low Dice index. In summary, the ICV difference between reference and study image should be small to yield a good ICV estimate for the study dataset.

In practice, one or more reference datasets should be chosen from a larger group by the method discussed above. Selection criteria are a low volume difference ($< 2\%$) and a high Dice index (> 0.96) for all adaptations in the group. The mean error may be used as an estimate for the expected error in the generation of the study ICV mask.

4 Discussion

A new approach for the determination of the intracranial volume in MRI datasets of the human head was described. In a nutshell, an ICV mask is computed from a high-resolution PD-weighted dataset. If such an image is not available, a non-linear registration between a T_1-weighted dataset of a reference and a study subject yields a deformation field that is applied to the reference PD-weighted dataset in order to obtain an artificial study PD-weighted dataset. An ICV mask for the study subject may then be generated. Using a suitable reference, this approach yields an expected volume error of less than 2% and an overlap of better than 0.97. The process is fully automatical and reliable: On a 4 processor cluster, we generated ICV masks for a database of 540 normal subjects in 68h.

Compared with the three approaches mentioned in the introduction, manual delineation of the intracranial cavity, as previously used in our [21], [22] and other studies [1], [7], [8], [10], [11], [18] is tedious (about 1.5h of work per dataset). If performed by an expert, it may still be considered as the gold standard, although small ambiguities due to the partial volume effect and inter-rater variability induce a volume error of the same magnitude as our method.

Alfano *et al.* [2], [3] suggested to use multispectral MRI datasets for ICV segmentation, while Lemieux *et al.* [15], [16] base their approach on T_1-weighted data only. Our method lies somewhat between both of these approaches: we use the helpful information provided by the PD-weighted datasets for ICV segmentation, but do not require that multispectral data are available for all subjects in a study. If high-resolution T_1-weighted data are provided, this method may even be used retrospectively.

As noted in the introduction, the ICV is closely related to the brain size of young healthy adults. Thus, ICV measures may be used to estimate the premorbid brain size, which is useful to compute the amount of atrophy in brain degeneration due to diffuse diseases (e.g., Alzheimer's disease, anoxic encephalopathy, microangiopathy) or following focal brain damage (e.g., cerebral infarction or hemorrhage, after tumor removal).

Acknowledgement

The authors wish to thank the MPI of Human and Cognitive Brain Science, Leipzig, for providing the datasets.

References

1. Abbott, A.H., Netherway, D.J., Niemann, D.B., Clark, B., Yamamoto, M., Cole, J., Hanieh, A., Moore, M.H., David, D.J.: CT-determined intracranial volume for a normal population. J Craniofac. Surg. **11** (2000) 211–223.
2. Alfano, B., Brunetti, A., Covelli, E.M., Quarantelli, M., Parnico, M.R., Ciarmiello, A., Salvatore, M.: Unsupervised, automated segmentation of the normal brain using a multispectral relaxometric magnetic resonance approach. Magn. Reson. Med. **37** (1997) 84–93.

3. Alfano, B., Quarantelli, M., Brunetti, A., Larobina, M., Covelli, E.M., Tedeschi, E., Salvatore, M.: Reproducibility of intracranial volume measurement by unsupervised multispectral brain segmentation. Magn. Reson. Med. **39** (1998) 497–499.
4. Andersen, A.H., Zhang, Z., Avison, M.J., Gash D.M.: Automated segmentation of multispectral brain MR images. J Neurosci. Meth. **122** (2002) 13–23.
5. Christensen, G.E.: Deformable shape models for anatomy. Thesis (1996) Washington University, St. Louis.
6. Dice, L.R.: Measures of the amount of ecologic association between species. Ecology **26** (1945) 297–302.
7. Edland, S.D., Xu, Y., Plevak, M., O'Brien, P., Tangalos, E.G., Petersen, R.C., Jack, C.R.: Total intracranial volume: normative values and lack of assiociation with Alzheimer's disease. Neurology **59** (2002) 272–274.
8. Eritaia, J., Wood, S.J., Stuart, G.W., Bridle, N., Dudgeon, P., Maruff, P., Velakoulis, D., Pantelis, C.: An optimized method for estimating intracranial volume from magnetic resonance images. Magn. Reson. Med. **44** (2000) 973–977.
9. Falkner, F.: Normal growth and development: current concepts. Postgrad. Med. **62** (1977) 58–63.
10. Hahn, F.J., Chu, W.K., Cheung, J.Y.: CT measurements of cranial growth: normal subjects. Am J Roentgenol. **142** (1984) 1253–1255.
11. Jenkins, R., Fox, N.C, Rossor, A.M., Harvey, R.J., Rossor, M.N.: Intracranial volume and Alzheimer disease. Arch. Neurol. **57** (2000) 220–224.
12. Kruggel, F., Lohmann, G.: BRIAN (Brain Image Analysis) - A toolkit for the analysis of multimodal brain data sets. In: Computer Aided Radiology (CAR'96) 323–328, Elsevier, Amsterdam.
13. Kruggel, F., von Cramon, D.Y.: Alignment of magnetic-resonance brain datasets with the stereotactical coordinate system. Med. Imag. Anal. **3** (1999) 1–11.
14. Lee, J.H., Garwood, M., Menon, R., Adriany, G., Andersen, P., Truwit, C.L., Ugurbil, K.: High contrast and fast three-dimensional magnetic resonance imaging at high fields. Magn. Reson. Med. **34** (1995) 308–312.
15. Lemieux, L., Hagemann, G., Krakow, K., Woermann, F.G.: Fast, accurate, and reproducible automatic segmentation of the brain and in T_1-weighted volume MRI data. Magn. Reson. Med. **42** (1999) 127–135.
16. Lemieux, L., Hammers, A., Mackinnon, T., Liu, R.S.N.: Automatic segmentation of the brain and intracranial cerebrospinal fluid in T_1-weighted volume MRI scans of the head, and its application to serial cerebral and intracranial volumetry. Magn. Reson. Med. **49** (2003) 872–884.
17. Pham, D.L., Prince, J.L.: An adaptive fuzzy segmentation algorithm of magnetic resonance images. IEEE T Med. Imag. **18** (1999) 737–752.
18. Sgouros, S., Hockley, A.D., Goldin, J.H., Wake, M.J., Natarajan, K.: Intracranial volume change in craniosynostosis. J Neurosurg. **91** (1999) 617–625.
19. Sgouros, S., Goldin, J.H., Hockley, A.D., Wake, M.J., Natarajan, K.: Intracranial volume change in childhood. J Neurosurg. **91** (1999) 610–616.
20. Tsao, Y.F., Fu, K.S.: A parallel thinning algorithm for 3D pictures. Comp. Graph. Imag. Proc. **17** (1981) 315–331.
21. Wolf, H., Kruggel, F., Hensel, A., Wahlund, L.O., Arendt, Th., Gertz, H.J.: The relationship between head size and intracranial volume in elderly subjects. Brain Res. **973** (2003) 74–80.
22. Wolf, H., Hensel, A., Kruggel, F., Riedel-Heller, S.G., Arendt, Th., Wahlund, L.O., Gertz, H.J.: Structural correlates of mild cognitive impairment. Neurobiol. Aging **25** (2004), in print.
23. Wollny, G., Kruggel, F.: Computational cost of non-rigid registration algorithms based on fluid dynamics. IEEE T Med. Imag. **21** (2001) 946–952.